Comparison of Confined, Compressible, Spatially Developing Mixing Layers with Temporal Mixing Layers

Linda Sigalla Hedges*
Boeing Commercial Airplane Group, Seattle, Washington 98124
and
D. Scott Eberhardt†
University of Washington, Seattle, Washington 98198

The spatially developing mixing layer is investigated using both linear stability theory and numerical simulations. Temporal and spatial linear stability solutions are compared, and it is found that the temporal and spatial wave numbers are equal, the temporal frequency is a function of the spatial frequency, and the temporal and spatial growth rates have a one-to-one correspondence. Numerical simulations of the Euler equations are performed for the spatially developing mixing layer using a linear stability forcing function. Spatially developing simulations of the supersonic/supersonic and supersonic/subsonic acoustic instabilities and the Kelvin-Helmholtz instability are compared to temporally developing simulations and found to be in agreement.

Nomenclature

a	= speed of sound
C_{ph}	= instability phase speed
D_c	= inverse Schmidt number
E	= perturbation kinetic energy
L	= characteristic length
M	= Mach number
M_c	= convective Mach number
p	= pressure $(p^*/\rho_\infty a_\infty^2)$
(S)	= spatial
(T)	= temporal
t	= time $(t^* a_\infty/L)$
U	= x-direction velocity component at the wall
u	= x-direction velocity component (u^*/a_∞)
v	= y-direction velocity component (v^*/a_∞)
α	= wave number
θ	= momentum thickness
π	= velocity, density, or pressure
ρ	= density (ρ^*/ρ_∞)
φ	= passive scalar
ω	= frequency

Subscripts

i	= imaginary component
r	= real component
1	= high-speed stream (upper stream)
2	= low-speed stream (lower stream)
∞	= freestream values
ave	= average

Superscripts

$\hat{\ }$	= eigenfunction
$'$	= perturbation
t	= transformed
$\bar{\ }$	= mean quantities
$*$	= dimensioned quantities

Introduction

HIGH Mach number shear layers play an important role in the development of supersonic combustion ramjet (scramjet) engines. Mixing of air and fuel in high-speed flows is hindered by both shorter combustor residence times and by stability of the supersonic shear layer relative to its subsonic counterpart. The physics behind compressible mixing is still poorly understood and requires much more experimentation. Experimentation, in the form of direct numerical simulation, can be costly unless one concentrates on the growth of selected instabilities in the temporal frame of reference. The use of temporally evolving simulations, however, is controversial since an idealized temporal shear layer can never be obtained in nature.

In this paper, we demonstrate that instabilities in the temporally developing mixing layer contain the same physical characteristics as in the spatially evolving mixing layer. The two models, temporal and spatial, are compared using both linear stability theory and numerical simulations for confined shear layers. The motivation is quite simple: temporally developing simulations require a significantly smaller computational grid. This enables greater structure resolution and shorter computer run times. Also, the temporal frame of reference employs periodic boundary conditions in the streamwise direction, which greatly simplifies the problem.

Viewed from a temporal frame of reference, a wave system grows in amplitude with respect to time. The temporal frame of reference is shown in Fig. 1. Viewed from a spatial frame of reference, a perturbation generates a train of waves that grow spatially as they travel away from the source. The spatial frame of reference is shown in Fig. 2. The temporal frame of reference is usually chosen to travel at the average velocity of the upper and lower streams of the equivalent spatial frame.

Gaster[1] compared the spatial and temporal frames of reference for small growth rate solutions. He found that, for weak amplification rates, temporally and spatially growing waves with the same wave number have equal frequencies, and their growth rates can be linked using the group velocity. In this paper, the linear stability relationship between the spatial and temporal frames of reference for all unstable solutions is investigated. Gaster's theorem coupled with a Galilean transformation demonstrates a one-to-one relationship between the temporal and spatial frames of reference. The structure of the resulting comparison is checked with the nonlinear numerical simulations.

The unconfined continuous flow profile has been studied with linear stability theory by many researchers.[2-8] Their re-
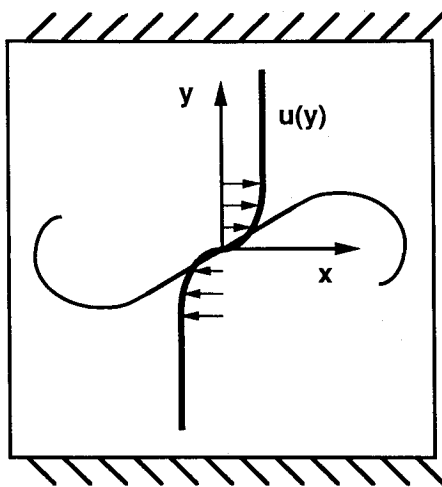
Fig. 1   Temporally developing mixing layer geometry.
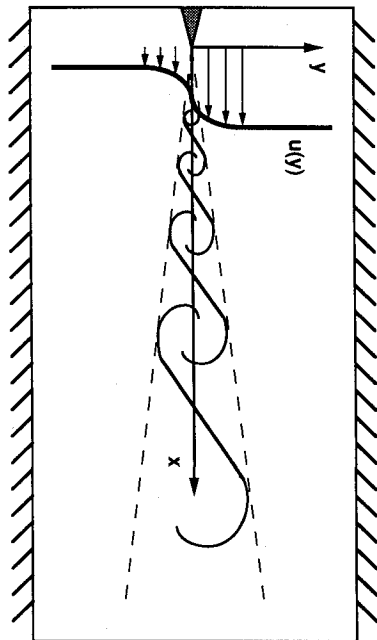
Fig. 2   Spatially developing mixing layer geometry.

sults show that unstable modes exist at all Mach numbers and that a decrease in mixing layer growth rate is seen with increasing freestream Mach number difference. The general features of the linear stability of supersonic mixing layers has been delineated by Jackson and Grosh.[7] They have shown that instability modes in the supersonic mixing layer convect at a variety of instability phase speeds, typically bounded by the speeds of the freestream velocities.

Jackson and Grosh have shown that the type of instability that arises in the confined, two-dimensional mixing layer is approximately determined by the convective Mach numbers of the high- and low-speed sides of the shear layer. The convective Mach numbers are the Mach numbers of each freestream relative to a frame of reference traveling with the large-scale structures. The convective Mach number of the high-speed stream is termed M_{c1}, and the convective Mach number of the low-speed stream is termed M_{c2}. The convective Mach numbers are defined as

$$M_{c1} = \frac{u_1 - C_{\text{ph}}}{a_1} \qquad M_{c2} = \frac{C_{\text{ph}} - U_2}{a_2} \qquad (1)$$

where U_1 and a_1 are the freestream velocity and speed of sound, respectively, in the high-speed stream, and U_2 and a_2

are similarly defined in the low-speed stream. The instability speed or the convective velocity of the large-scale coherent structure is C_{ph}.

The type of instability that arises in two-dimensional mixing layers is determined by the convective Mach numbers defined in Eq. (1). When the convective Mach numbers M_{c1} and M_{c2} are both less than one, then the instability is a Kelvin-Helmholtz (subsonic) instability. When the convective Mach number with respect to one or both of the streams is greater than one, then the instability is an acoustic (supersonic) instability.

The acoustic instabilities are subclassified as supersonic/supersonic (or doubly supersonic) and supersonic/subsonic. The type of instability is again defined by the convective Mach numbers. When the convective Mach numbers are both greater than one, then the instability is a supersonic/supersonic instability. When the convective Mach number with respect to one but not both of the freestreams is less than one, then the instability is a supersonic/subsonic instability. Furthermore, if the instability travels at a velocity closer to the higher velocity stream, then the instability is called a fast supersonic/subsonic mode. Conversely, if the instability travels with a velocity closer to the lower velocity stream, then the instability is called a slow supersonic/subsonic mode.

Numerical simulations have also captured the effects of compressibility on unbounded mixing layers. A good comparison between numerical simulation results and experimental observation was achieved by Soetrisno[9] and Soetrisno et al.[10] for unbounded, temporal, supersonic mixing layers. The three-dimensional, unconfined, compressible mixing layer was investigated in the temporal frame of reference by Sandham and Reynolds.[11]

More recently, linear stability analysis of the supersonic mixing layer has included the effect of walls. Tam and Hu[12] investigated the confined, spatially developing, compressible mixing layer, and Greenough et al.[13] investigated the confined, temporally developing, compressible mixing layer. Both demonstrated the existence of acoustic modes for convective Mach numbers greater than one. The confined mixing layers were shown to be much more unstable than the unconfined mixing layers. The existence of acoustic modes was discovered by Gill[14] for shear layers and Mack[15] for boundary layers. The acoustic instability was shown to be the result of waves bouncing between the wall and the sonic line.

Numerical simulation of the confined acoustic modes was performed temporally by Soetrisno et al.[16,17] and Soetrisno[18] who investigated a variety of two- and three-dimensional nonlinear Kelvin-Helmholtz and acoustic instabilities and their interactions within the temporal mixing layer. The work characterized the large-scale coherent structure, mixing behavior, and energetics of the different individual instability types. The work also demonstrated that there are strong interactions between the two- and three-dimensional instabilities.

In two dimensions, Sigalla et al.[19] simulated the acoustic instabilities in the confined, spatially developing mixing layer. Ragab and Sheen[20] and later Wu[21] have also simulated individual acoustic modes in spatially developing mixing layers. Sigalla et al.[22] have demonstrated the broadbanded nature of the acoustic instability and determined the importance of interacting acoustic modes in understanding the supersonic mixing layer. Huang and Riley[23] have further explored the three-dimensional temporally developing mixing layer with broadbanded white noise forcing.

Many of these past studies have focused on understanding how unstable modes grow in a compressible shear layer. Much has been learned by visualizing the structure of these unstable modes. Here, we will demonstrate that the structure of an unstable mode in the temporal shear layer is characteristically the same as in a spatial shear layer.

Linear Stability Comparison

Linear stability theory provides a method for predicting which perturbations are most likely to grow in a shear layer.

Eigenfunction solutions then determine the forcing function necessary to excite a given instability or group of instabilities in a numerical simulation. Linear stability theory can also be used to help validate a numerical simulation by providing predictions for shear layer growth rate, coherent structure wavelength, and phase speed, against which the linear portion of the numerical solution can be compared.

Linear Stability Methodology

The temporal linear stability analysis used here is discussed in Greenough et al.,[13] and the spatial linear stability code is discussed in Huang and Riley.[23] Briefly, the continuous profile problem is solved for flow in a channel. The fluid is assumed to be inviscid, nonheat conducting, and adiabatic. The uniform flow conditions are perturbed and substituted into the governing equations. Linearizing these equations and assuming a normal mode formulation gives a system in the form of a nonlinear eigenvalue problem. The equations are solved both spatially and temporally.

The normal mode formulation for the perturbation is expressed as

$$\pi' = Re\{\hat{\pi}(y)e^{i(\alpha x - \omega t)}\}$$

where π represents either pressure, velocity, or density. The perturbation from the mean flow is represented by π', and the complex eigenfunctions are represented by $\hat{\pi}$. In general, both α and ω are complex. However, the temporal instability grows only in time, and thus α is purely real. Spatially, the instability grows only in downstream distance, and thus ω is purely real. Physically, α_r represents the length of the large-scale coherent structure and ω_r the frequency at which a splitter plate would be oscillated to force that particular instability. The spatial

a) **Wavenumber (α_r)**

b) **Wavenumber (α_r)**
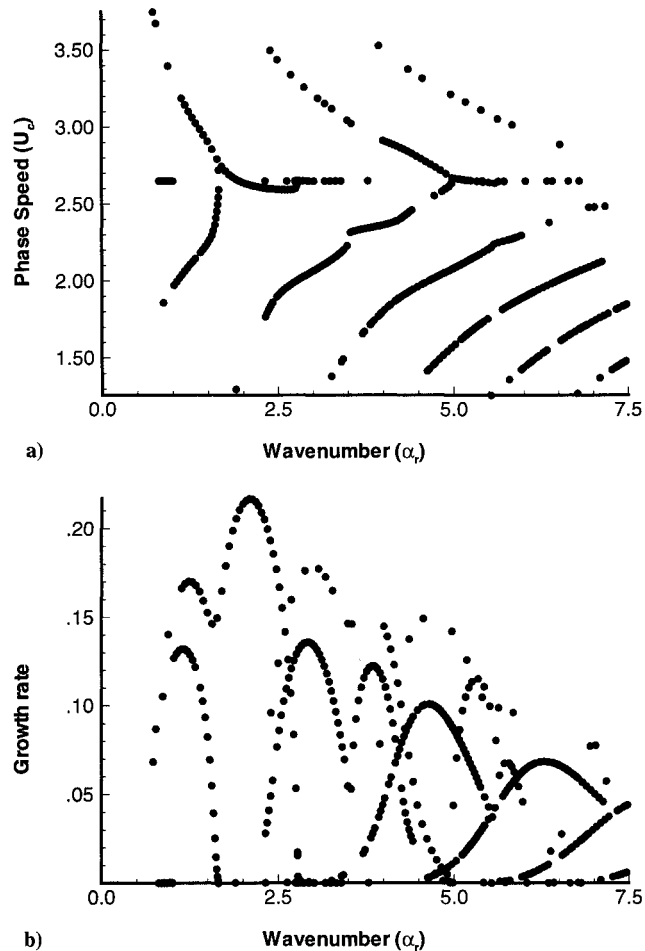
Fig. 3 Spatial phase speed and growth rate, $M_1 = 4.1$, $M_2 = 1.2$; a) C_{ph} vs α_r and b) $-\alpha_i$ vs α_r.

a) **Wavenumber (α_r)**

b) **Wavenumber (α_r)**
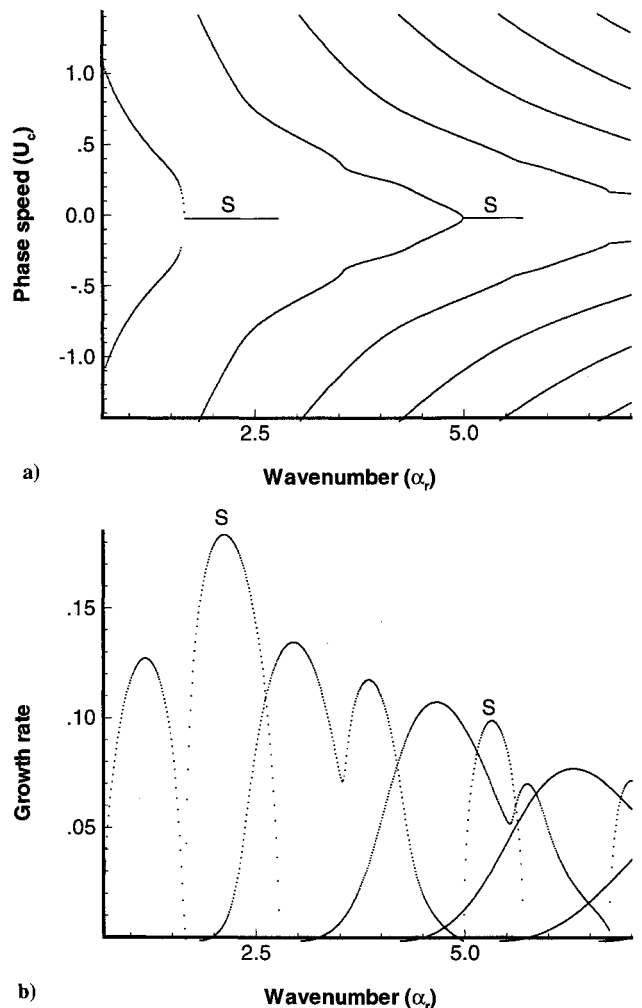
Fig. 4 Temporal phase speed and growth rate, $M_1 = 1.45$, $M_2 = -1.45$; a) C_{ph} vs α_r and b) ω_i vs α_r.

growth rate is given by $-\alpha_i$ and the temporal growth rate is given by ω_i. The phase speed of the instability C_{ph} is given by

$$C_{ph} = (\omega_r / \alpha_r) \qquad (2)$$

Linear Stability Results

The temporal and spatial linear stability solutions are correlated with the following relations:

$$\alpha_r(S) = \alpha_r(T)$$

$$\omega_r(S) = \omega_r(T) + \alpha_r(T) \times \bar{U}(S)$$

$$-\alpha_i(S) = (\omega_i / U_g)(T) \qquad (3)$$

where $\bar{U}(S)$ is the average of the spatial freestream velocities and U_g is the group velocity given by

$$U_g = -\frac{d\omega_r}{d\alpha_r} \qquad (4)$$

The spatial and temporal group velocities are approximately equal. T denotes a temporal value, and S denotes a spatial value. Since the spatial and temporal wave numbers are equivalent, they will both be referred to as α_r. Since α_i only occurs in the spatial frame of reference and ω_i only occurs in the temporal frame of reference, their frames of reference will not be denoted.

When the spatial and temporal frames of reference are compared with these relationships, the two solutions fall on top of one another. The significance of this is that, for every
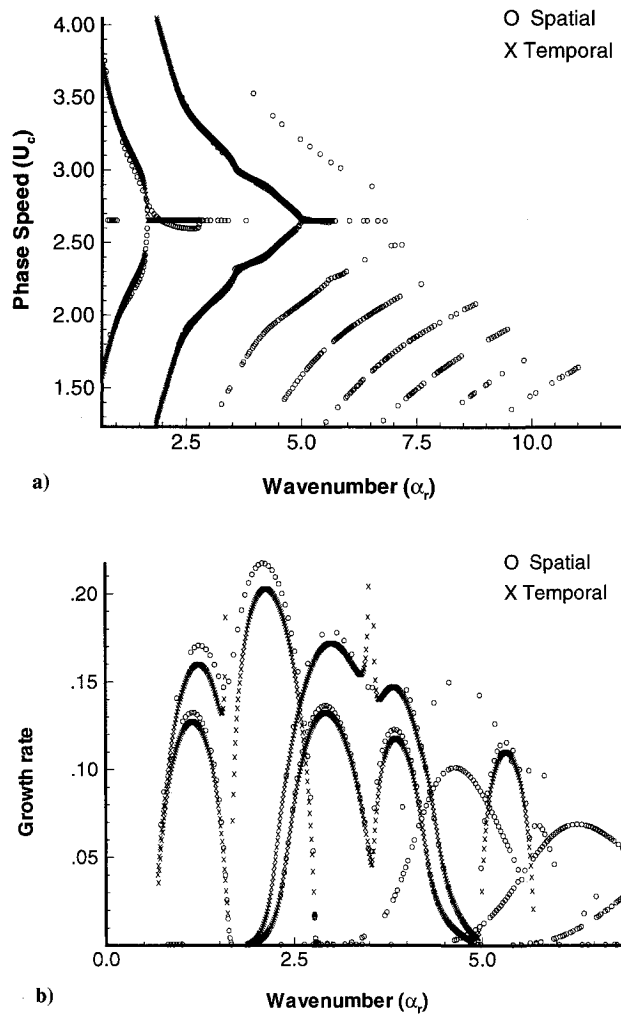
Fig. 5 Comparison of temporal and spatial phase speed and growth rate; a) C_{ph} vs α_r and b) $-\alpha_i$ vs α_r.

temporal wave number α_r, there is an equal spatial wave number α_r and a corresponding frequency $\omega_r(S)$, with correspondence between the temporal and spatial growth rates.

Figure 3 shows a plot of the spatial stability solutions for a Mach number difference of $\Delta M = 2.9$. The freestream Mach numbers are $M_1 = 4.1$ and $M_2 = 1.2$. Figure 3a is a plot of the spatial phase speed vs wave number. Figure 3b is a plot of the spatial growth rate vs wave number.

The corresponding plot of the temporal stability solutions for the same Mach number difference is shown in Fig. 4. The freestream Mach numbers are $M_1 = 1.45$ and $M_2 = -1.45$. Figure 4a is a plot of the temporal phase speed vs wave number. Figure 4b is a plot of the temporal growth rate vs wave number. The temporal stability solutions have the property that they are either symmetric or asymmetric. The symmetric modes have zero phase speed, and are indicated with an S in Fig. 4. The asymmetric modes have nonzero phase speeds and come in pairs. Referring to Fig. 4a, each point on an asymmetric branch has a corresponding point on an opposite branch with an equal growth rate and an equal but opposite phase speed. Thus, the asymmetric growth rate peaks shown in Fig. 4b are actually two peaks, one on top of the other.

Figure 5a shows the spatial phase speed superimposed on the predicted spatial phase speed determined from the temporal solutions and Eqs. (3). The solutions lie almost exactly one on top of the other, demonstrating the equivalence of the wave numbers α_r and the correspondence of the phase speeds C_{ph}. A small discrepancy shows up at the location of the temporal symmetric modes. This is because spatial symmetric modes are not possible and so the frequencies are off by a few percent.

Agreement is also seen at a Mach number difference of $\Delta M = 2$.

Figure 5b is a plot of the spatial growth rate superimposed on the predicted spatial growth rate from the temporal solutions and Eqs. (3). The temporal asymmetric growth rate peaks no longer fall one on top of the other, but again there is a one-to-one temporal/spatial correspondence.

These figures show that, through the application of linear stability theory, the temporal and spatial wave number, phase speed, and growth rate are in good agreement.

Numerical Simulation Comparison

Numerical Method

The numerical simulations solve the two-dimensional, non-steady Euler equations governing the motion of inviscid, non-heat-conducting gases. The Euler equations are written in conservation law form so that any shock waves and contact surfaces are captured as part of the solution. The second-order, total variation diminishing (TVD) algorithm by Yee et al.[24] is used with Runge-Kutta time advancement.

The mean flow is initialized with the dimensionless mean flow properties $\bar{\rho} = 1$ and $\bar{p} = 1/\gamma$, and the velocity profile is given by

$$ u = \left(\frac{U_1 + U_2}{2}\right)\left[1 + \left(\frac{U_2 - U_2}{U_1 + U_2}\right) \tanh\left(\frac{y}{2}\right)\right] $$

with $v = 0$. Here U_1 and U_2 are the upper and lower stream velocities at the walls. The momentum thickness is 0.05 and the channel halfwidth L (the characteristic length) is always 1. For this paper, the channel is always considered to be symmetric.

A periodic forcing function (obtained from linear stability theory) given by

$$ \pi' = \hat{\pi}_r(y) \cos(\omega_r t) + \hat{\pi}_i(y) \sin(\omega_r t) $$

is applied continually at the end of the splitter plate. The perturbation is added to the basic state inflow conditions for the upstream boundary condition. The outflow boundary condition is based on the flow characteristics in the streamwise direction. Free-slip, nonpermeable wall boundary conditions are used in the transverse direction.

The fundamental difference between the numerical simulation of the spatial and temporal shear layers lies in the application of the boundary conditions and of the instability perturbation. The temporal inflow-outflow boundary conditions are periodic, and the temporal perturbation is added only once to the initial condition. Note that this boundary condition implies that the solution domain in the streamwise direction is equal to the wavelength of the initial perturbation (or an exact multiple of it). Thus, the solution domain changes for each instability mode considered. Also, when more than one mode is present the domain size must be an exact multiple of both wave numbers.

The spatial computational domain is a rectangle containing 400×67 equally spaced grid points, corresponding to a domain size of dimensionless length 2×20. Each simulation was allowed to flow through twice at the average velocity of the two streams. The amplitude of the perturbation was chosen to be 5%, with a Courant-Fredrichs-Lewy (CFL) number of 0.2 to ensure numerical stability and to resolve the time evolution. The spatial geometry does not have to change for each instability considered as in the temporal simulations. Also, the streamwise length does not have to be an exact multiple of each wavelength if more than one mode is present.

To better understand the entrainment processes in the shear layers, a passive scalar field is introduced. The passive scalar serves to "tag" the incoming streams, so that the evolution of each stream may be tracked separately. The evolution of this

passive scalar is governed by the time-dependent advection equation:

$$\frac{\partial \varphi}{\partial t} + u \cdot \nabla \varphi = D_c \nabla^2 \varphi$$

The passive scalar represents a fast, equimolecular, irreversible reaction. The mixing product concentration obtained from the passive scalar gives a good indication of mixing characteristics in the computed shear layers. Since this equation is decoupled from the fluid dynamical equations, the

Table 1 Instability modes simulated for spatial to temporal comparison

Case	M_1	M_2	ΔM	Instability type	α_r	$C_{ph}(S)$	$C_{ph}(T)$	$-\alpha_i$	ω_i
1	4.1	1.2	3.0	Sup/sup	2.13	2.62	0.0	-0.22	0.39
2	6.0	3.1	3.0	Sup/sup	2.13	4.54	0.0	-0.12	0.39
3	3.2	1.2	2.0	Slow sup/sub	2.65	2.0	-0.19	-0.17	0.50
4	3.0	1.5	1.5	Kelvin-Helmholtz	2.99	2.25	0.0	-0.29	1.3

a)

b)
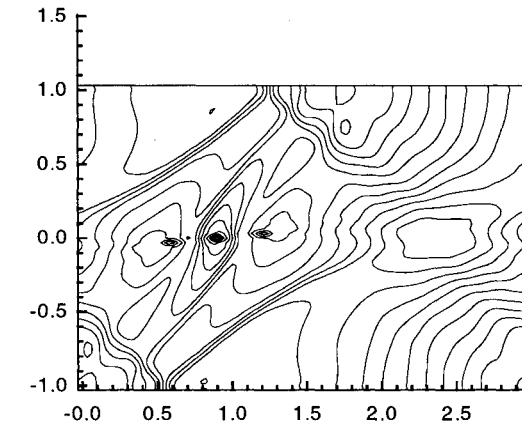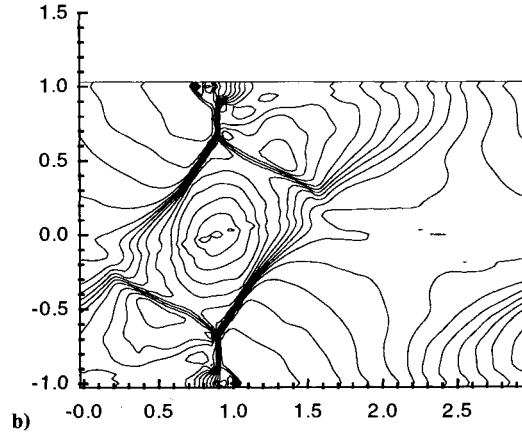
Fig. 6 Temporal density contours for the supersonic/supersonic instability; a) $t = 20$ and b) $t = 30$.


a)

b)
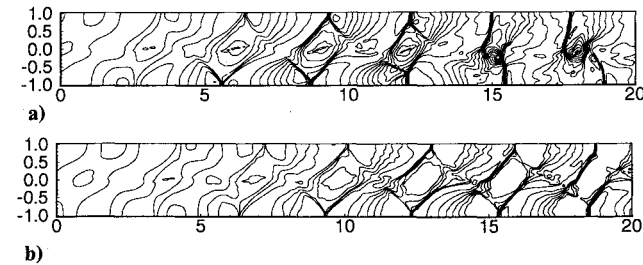
Fig. 7 Spatial density contours for the supersonic/supersonic instability; a) $M_1 = 4.1$ and b) $M_1 = 6$.


a)

b)
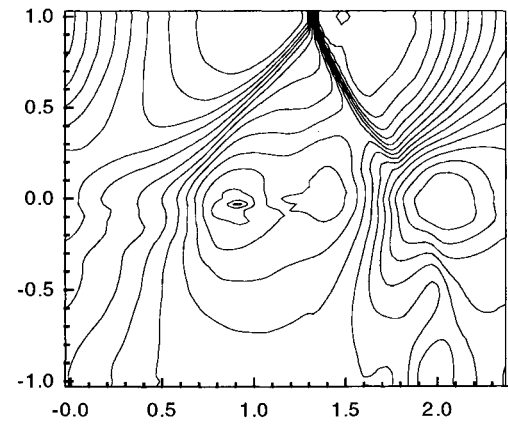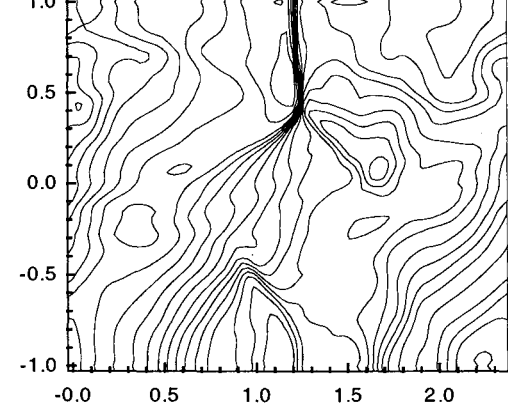
Fig. 8 Temporal density contours for the supersonic/subsonic instability; a) $t = 16$ and b) $t = 30$.

scalar field is guaranteed to be "passive," and only acts as a fluid marker. The advection equation is solved using a Lax-Wendroff scheme.

Details of the numerical scheme, boundary conditions, initial conditions, and passive scalar field can be found in Refs. 18 and 25.

Numerical Results

In this section, spatial simulations are compared to temporal simulations to determine the relationship between the nonlinear instability structure in the two frames of reference. The Mach number differences simulated are the same as those presented for the temporal simulations in Soetrisno.[18] Three Mach number differences were compared, corresponding to each instability type: supersonic/supersonic, supersonic/subsonic, and Kelvin-Helmholtz. For the supersonic/supersonic instability comparison, two spatial simulations were run at the same Mach number difference but with different freestream Mach numbers. The four comparison cases are shown in Table 1. The temporal simulations are provided by Soetrisno.[18]

Density contours of the temporal supersonic/supersonic instability ($\Delta M = 2.9$) are shown in Fig. 6. This is the temporal simulation for comparison with the spatial simulation cases 1 and 2. Figure 6a shows the temporal simulation at a time just after saturation, and Fig. 6b shows the temporal simulation at a time well past saturation.

Spatial simulation cases 1 and 2 ($\Delta M = 2.9$) are shown in Fig. 7. Case 1 (Fig. 7a) has freestream Mach numbers $M_1 = 4.1$ and $M_2 = 1.2$. Case 2 (Fig. 7b) has freestream Mach numbers $M_1 = 6$ and $M_2 = 3.1$. The phase speed is zero in the temporal simulation, and the phase speeds are $C_{ph} = 2.62$ (case 1) and $C_{ph} = 4.54$ (case 2) for the spatial simulations. Converting the temporal phase speed to the spatial frame of reference shows a difference in the phase speeds of 1.1 and 0.2%.

The spatial mixing layer in case 1 has a growth rate almost double that of the mixing layer in case 2. Thus, case 1 (Fig. 7a) shows earlier saturation with downstream distance and has more quickly changing structure shapes than case 2 (Fig. 7b).

The temporal structures compare quite well with the spatial structures. For instance, the temporal structure appearing in Fig. 6a is comparable to the case 1 spatial structure in Fig. 7a at about $x = 7$, and to the case 2 spatial structure in Fig. 7b at about $x = 10.5$. The temporal structure appearing in Fig. 6b is comparable to the case 1 spatial structure in Fig. 7a at about $x = 12$, and to the case 2 spatial structure in Fig. 7b at about $x = 17$.

Case 3 is a comparison of the supersonic/subsonic instability for $\Delta M = 2$. The temporal density contours are shown in Fig. 8. Figure 8a is at a time just after saturation, whereas Fig. 8b is at a time well past saturation. The spatial comparison is shown in Fig. 9. The freestream Mach numbers are $M_1 = 3.2$ and $M_2 = 1.2$. The temporal phase speed is $C_{\mathrm{ph}} = -0.19$. The spatial phase speed is $C_{\mathrm{ph}} = 2$. Transforming the temporal
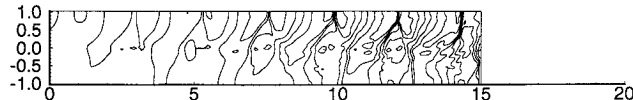

Fig. 9 Spatial density contours for the supersonic/subsonic instability, $M_1 = 3.2$.


a)

b)
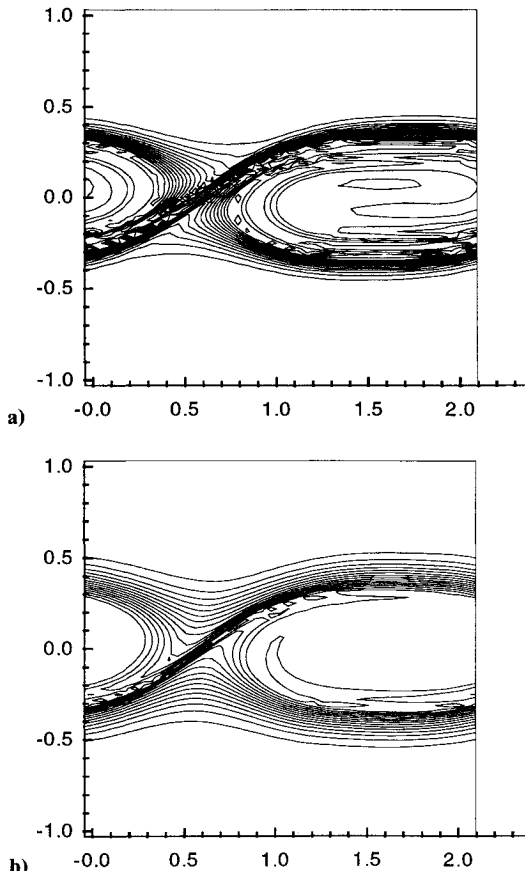
Fig. 10 Temporal passive scalar contours for the Kelvin-Helmholtz instability; a) $t = 24$ and b) $t = 30$.
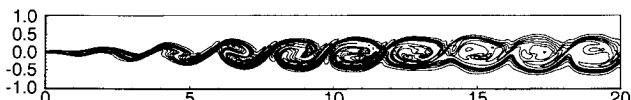
Fig. 11 Spatial passive scalar contours for the Kelvin-Helmholtz instability, $M_1 = 3$.

phase speed to the spatial frame of reference shows a difference of 0.5%.

The temporal structures compare well to the spatial structures. For instance, the temporal structure appearing in Fig. 8a is comparable to the spatial structure in Fig. 9 at about $x = 7$. The temporal structure appearing in Fig. 8b is comparable to the spatial structure in Fig. 9 at about $x = 13$.

Case 4 is a comparison of the Kelvin-Helmholtz instability with $\Delta M = 1.5$. Passive scalar contours are shown in Fig. 10. The corresponding passive scalar contours for the spatial mixing layer with freestream Mach numbers $M_1 = 3$ and $M_2 = 1.5$ are shown in Fig. 11.

Again the temporal structures compare well to the spatial structures. For instance, the temporal structure appearing in Fig. 10a is comparable to the spatial structure in Fig. 11 at about $x = 8$. The temporal structure appearing in Fig. 10b is comparable to the spatial structure in Fig. 11 at about $x = 14$.

Conclusions

The spatially developing shear layer was investigated using both linear stability theory and numerical simulations. The temporal and spatial linear stability solutions were compared to each other and found to have almost exact agreement. It was found that for every spatial wave number $\alpha_r(S)$ there is an equal temporal wave number $\alpha_r(T)$ corresponding to the same type of instability. The spatial frequency $\omega_r(S)$ is related to the temporal frequency $\omega_r(T)$ through α_r and the average of the spatial shear layer velocities U_{ave}. It was also found that the temporal growth rate ω_i is related to the spatial growth rate α_i through the temporal phase speed and U_{ave}.

Numerical simulations of the Euler equations were performed for the spatially developing shear layer using linear stability perturbations for the upstream boundary conditon. Supersonic/supersonic and supersonic/subsonic acoustic instabilities and Kelvin-Helmholtz instabilites were found with the spatial simulations. These simulations were compared to previous temporal simulations at the convective Mach numbers $M_c = 1.45$, 1.0, and 0.75. The structures of the instabilities were found to be in good agreement for all cases.

The temporally developing shear layer has been demonstrated to be a meaningful tool for studying instability growth in the confined shear layer. Most important, however, is that this work gives credibility to the conclusions drawn from the numerous temporal shear layer studies discussed in the Introduction. A great deal of insight at reduced computational cost has been gained by exploiting the temporal model.

Although a good model for isolated instability growth, the temporal geometry is not an economical model for simulating an instability resulting from interacting unstable modes. As mentioned previously, to satisfy the boundary conditions the temporal domain must be large enough to contain a whole number of both modal wavelengths. The temporal simulations are also unable to capture the growth of nonmultiple wavelength modes that are excited by the nonlinear interactions. Work that stresses the nonlinear interaction of instability modes, therefore, must employ the spatial geometry.

Acknowledgment

References

[1]Gaster, M., "A Note on the Relation Between Temporally Increasing and Spatially Increasing Disturbances in Hydrodynamic Stability," *Journal of Fluid Mechanics*, Vol. 14, Pt. 2, 1962, pp. 222–224.

[2]Lees, L., and Lin, C. C., "Investigation on the Stability of the Laminar Boundary Layer in Compressible Fluid," NACA-TN-1115, 1946.

[3]Blumen, W., "Shear Layer Instability of an Inviscid Compressible Fluid," *Journal of Fluid Mechanics*, Vol. 40, Pt. 4, 1970, pp. 769–781.

[4]Blumen, W., Drazin, P. G., and Billings, D. F., "Shear Layer Instability of an Inviscid Compressible Fluid, Part 2," *Journal of*

Fluid Mechanics, Vol. 71, Pt. 2, 1975, pp. 305–316.

[5]Drazin, P. G., and Davy, A., "Shear Layer Instability of an Inviscid Compressible Fluid, Part 3," *Journal of Fluid Mechanics,* Vol. 82, Pt. 2, 1977, pp. 255–260.

[6]Ragab, S. A., and Wu, J. L., "Linear Instability Waves in Supersonic Turbulent Mixing," AIAA Paper 87-1418, June 1987.

[7]Jackson, T. L., and Grosch, C. E., "Inviscid Spatial Stability of a Compressible Mixing Layer," *Journal of Fluid Mechanics,* Vol. 208, Nov. 1989, pp. 609–637.

[8]Ragab, S. A., and Wu, J. L., "Instabilities in Free Shear Layers Formed by Two Supersonic Streams," AIAA Paper 88-0038, Jan. 1988.

[9]Soetrisno, M., "A Study of Inviscid Supersonic Mixing Layer Using a Second-Order TVD Scheme," M. S. Thesis, Dept. of Aeronautics and Astronautics, Univ. of Washington, Seattle, WA, Dec. 1987.

[10]Soetrisno, M., Eberhardt, D. S., Riley, J. J., and McMurtry, P. A., "A Study of Inviscid Supersonic Mixing Layer Using a Second-Order TVD Scheme," *AIAA Journal,* Vol. 27, No. 12, 1988, pp. 1770–1778; also AIAA Paper 88-3676, July 1988.

[11]Sandham, N., and Reynolds, W., "The Compressible Mixing Layer: Linear Theory and Direct Simulation," AIAA Paper 89-0371, Jan. 1989.

[12]Tam, C. K. W., and Hu, F. Q., "The Instability and Acoustic Wave Modes of Supersonic Mixing Layers Inside a Rectangular Channel," *Journal of Fluid Mechanics,* Vol. 203, June 1989, pp. 51–76.

[13]Greenough, J. A., Riley, J. J., Soetrisno, M., and Eberhardt, D. S., "The Effects of Walls on a Compressible Mixing Layer," AIAA Paper 89-0372, Jan. 1989.

[14]Gill, A. E., "Instabilities of 'Top-Hat' Jets and Wakes in Compressible Fluids," *Physics of Fluids,* Vol. 8, No. 8, 1965, pp. 1428–1430.

[15]Mack, L. M., "Boundary Layer Stability Theory," AGARD Rept. R-709, 1984.

[16]Soetrisno, M., Greenough, J. A., Eberhardt, D. S., and Riley, J. J., "Confined Compressible Mixing Layers: Part I. Three-Dimensional Instabilities," AIAA Paper 89-1810, June 1989.

[17]Soetrisno, M., Eberhardt, D. S., Greenough, J. A., and Riley, J. J., "Confined Compressible Mixing Layers: Part II. 3D Kelvin-Helmholtz—2D Kelvin-Helmholtz Interactions," AIAA Paper 90-1466, June 1990.

[18]Soetrisno, M., "Numerical Simulations of Temporally Developing, Confined Compressible Shear Layers," Ph.D. Dissertation, Dept. of Aeronautics and Astronautics, Univ. of Washington, Seattle, WA, June 1990.

[19]Sigalla, L. A., Eberhardt, D. S., Greenough, J. A., Riley, J. J., and Soetrisno, M., "Numerical Simulation of Confined, Spatially-Developing Mixing Layers: Comparison to the Temporal Shear Layer," AIAA Paper 90-1462, June 1990.

[20]Ragab, S. A., and Sheen, S., "Numerical Simulation of a Compressible Mixing Layer," AIAA Paper 90-1669, June 1990.

[21]Wu, K., "Numerical Investigation of Confined Supersonic Mixing Flow," Ph.D. Dissertation, National Cheng Kung Univ., Inst. of Aeronautics and Astronautics, Tainan, Taiwan, June 1991.

[22]Sigalla, L. A., Eberhardt, D. S., and Riley, J. J., "Numerical Simulation of Compressible, Confined, Spatially Developing Shear Layers: Nonlinear Interactions Between Instability Modes," AIAA Paper 91-1643, June 1991.

[23]Huang, H., and Riley, J. J., "Transition to Turbulence in Confined Compressible Mixing Layers: Part I. Three-Dimensional Simulations with Excitations of Random Broadbanded Noise," AIAA Paper 92-0553, Jan. 1992.

[24]Yee, H. C., Warming, R. F., and Harten, A., "Implicit Total Variation Diminishing (TVD) Schemes for Steady State Calculations," *Journal of Computational Physics,* Vol. 57, No. 3, 1984, pp. 327–360.

[25]Sigalla Hedges, L., "Numerical Simulation of the Acoustic Instability in the Spatially Developing, Confined, Supersonic, Mixing Layer," Ph.D. Dissertation, Dept. of Aeronautics and Astronautics, Univ. of Washington, Seattle, WA, Dec. 1991.